Supplementary Information for

Artificial inflation of apparent photocatalytic activity induced by catalyst-mass-normalization and a method to fairly compare heterojunction systems

Larissa Y. Kunz,[a] Benjamin T. Diroll,[b] Cody J. Wrasman,[a] Andrew R. Riscoe,[a] Arun Majumdar,[c] Matteo Cargnello[a,*]

[a]*Department of Chemical Engineering and SUNCAT Center for Interface Science and Catalysis, Stanford University, Stanford, CA 94305, USA*

[b]*Center of Nanoscale Materials, Argonne National Laboratory, Lemont, IL 60439, USA*

[c]*Department of Mechanical Engineering and Precourt Institute for Energy, Stanford University, Stanford, CA 94305, USA*

E-mail: mcargnello@stanford.edu

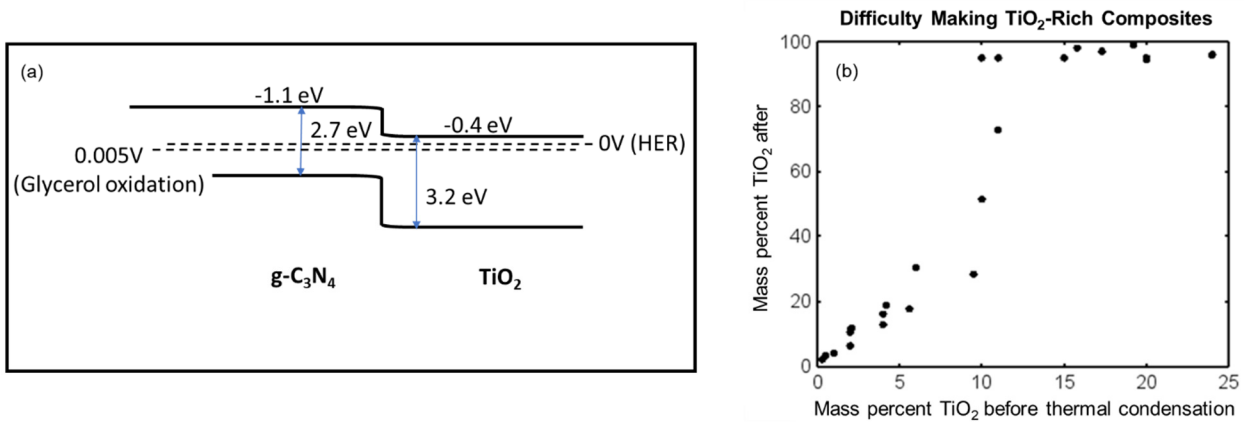

Figure S1. (a) Band diagram of a g-C_3N_4/TiO_2 heterojunction, based on bulk material properties; (b) graph of the mass percent of TiO_2 in the TiO_2/g-C_3N_4 composite (after thermal condensation, as measured by thermogravimetric analysis) versus in the TiO_2/dicyandiamide mixture (before thermal condensation of dicyandiamide to g-C_3N_4).

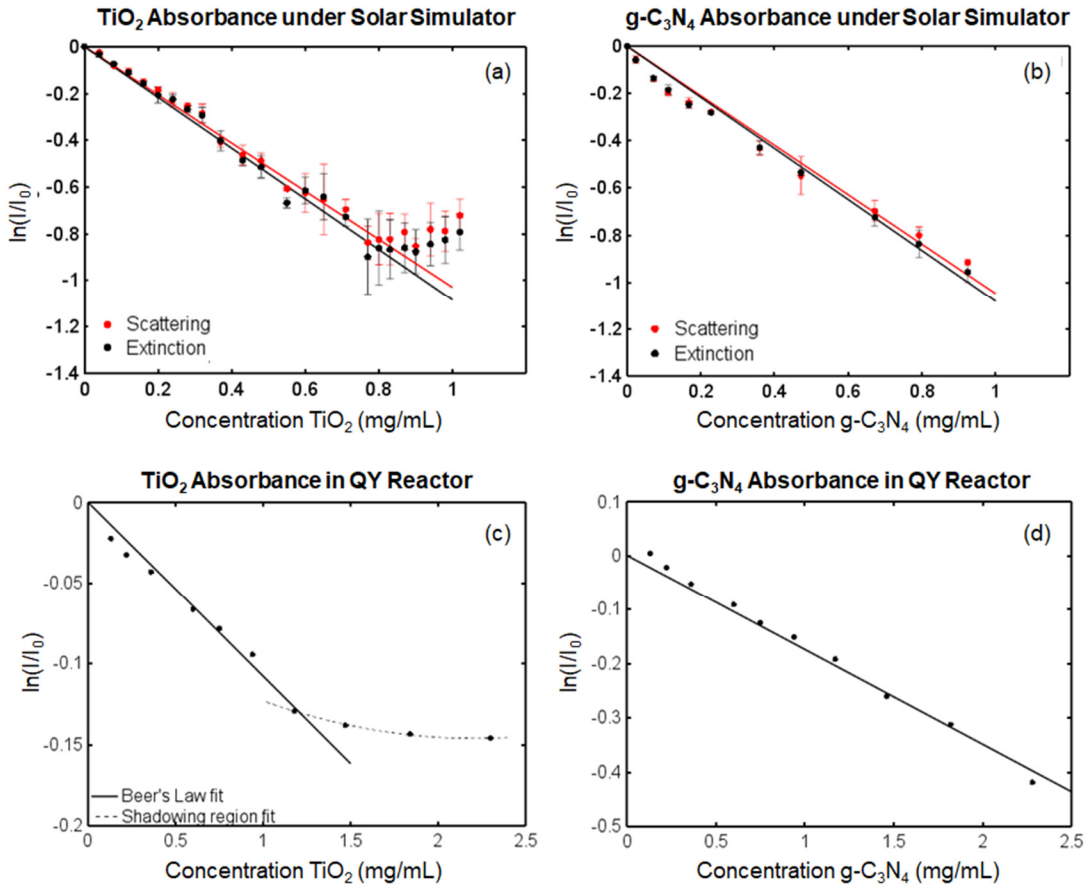

Figure S2. Fitting of Beer's law to light transmission data (plotted as the log of the outgoing over ingoing intensity, (I/I0)) under reaction conditions (using simulated solar light) for TiO_2 (a,c) and g-C_3N_4 (b,d) under the solar simulator (a,b) and in the quantum yield reactor (c,d). Under the solar simulator, extinction coefficients were measured using the full simulated AM1.5 spectrum while the scattering coefficient was determined using (a) a 385 nm longpass filter and (b) a neutral density NG1 filter to remove absorption by TiO_2 and g-C_3N_4 respectively. Absorption coefficients could be directly measured in-situ in the QY reactor by means of the incorporated integrating sphere.

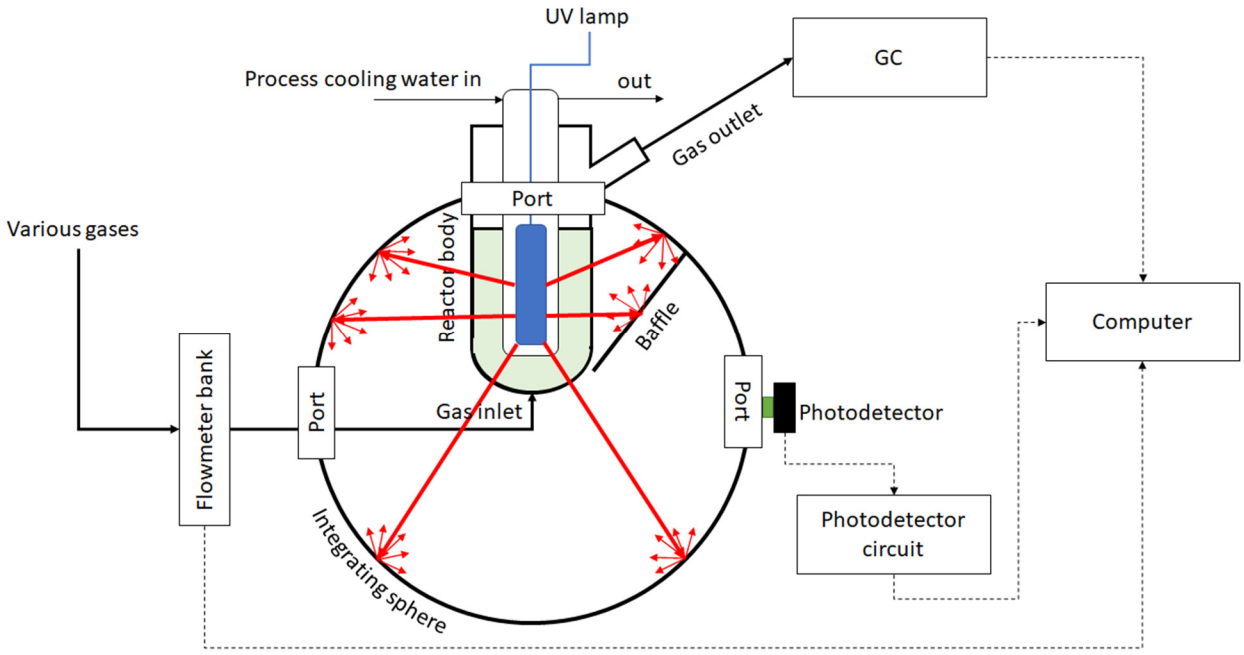

Figure S3. Experimental setup used to directly measure quantum yields at 365 nm. Solid black lines represent material flows, dotted lines represent information flows, and red lines portray representative light paths from the UV lamp and the ensuing diffuse reflectance off of the surface of the integrating sphere. The baffle blocks direct paths between the lamp and the photodetector, so only reflected light reaches the photodetector.

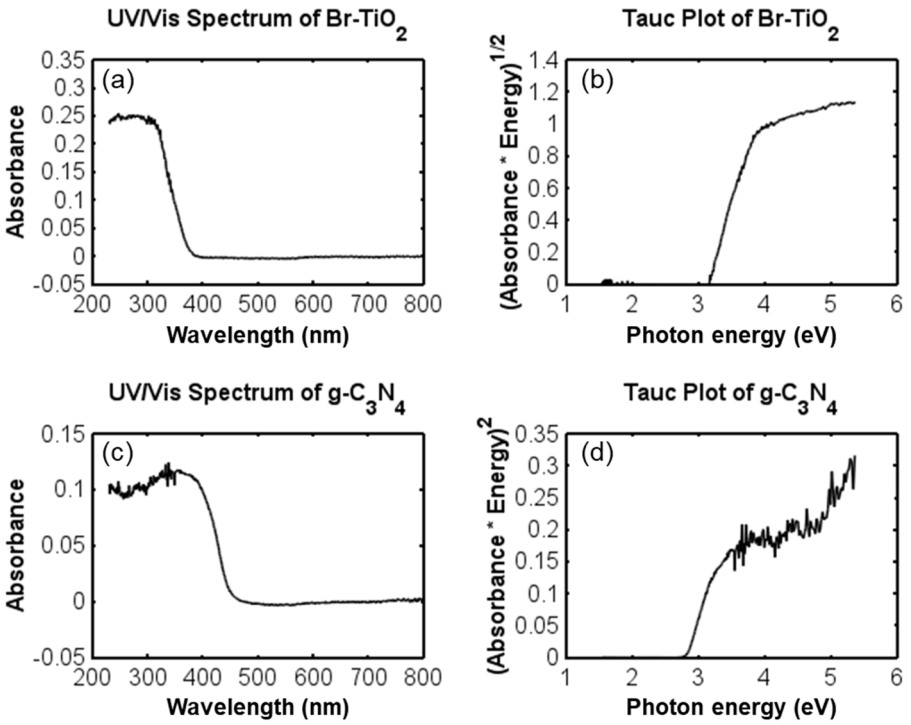

Figure S4. UV/Vis spectra (a,c) and their associated Tauc plots (b,d) for thermally treated br-TiO_2 nanorods (a,b) and g-C_3N_4 (c,d) dispersed in water. Note that the band gap extrapolated from (d), about 2.8 eV, is slightly larger than the 2.7 eV band gap from the solid-state measurement in Figure S2d - likely because smaller particles with fewer layers of sheets, showing quantum confinement effects, are more easily dispersible than large particles.

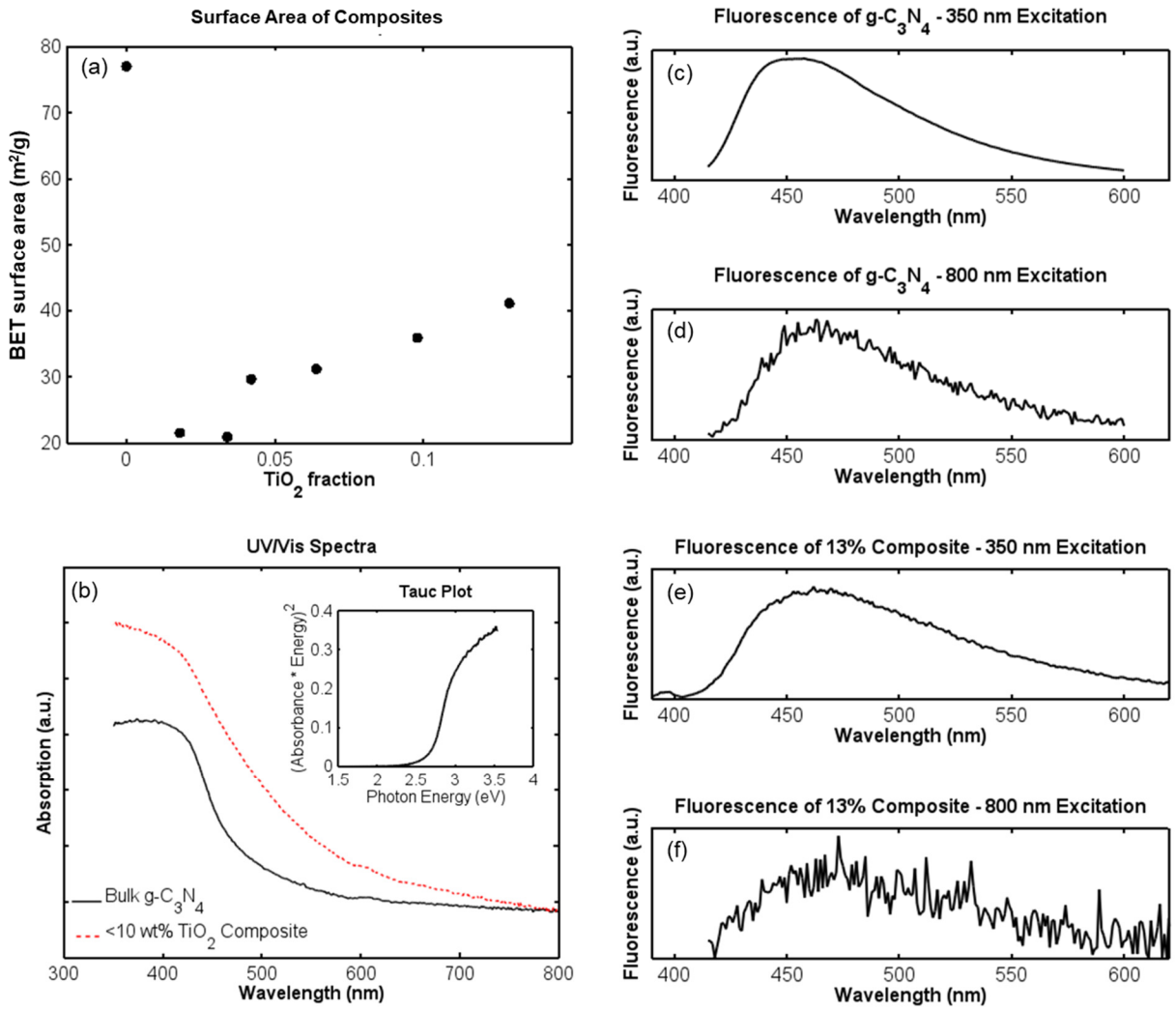

Figure S5. Supplementary characterization, including (a) BET surface area of g-C_3N_4 and low TiO_2 weight loading composites; (b) UV/Vis spectra of g-C_3N_4 and a composite (in their solid states) with inset Tauc plot indicating a g-C_3N_4 band gap of ~2.7 eV; and (c) corrected fluorescence spectra with single-photon excitation (350 nm) and (d) two-photon excitation (800 nm, with lower signal-to-noise) of the bulk g-C_3N_4 and (e-f) of the composites.

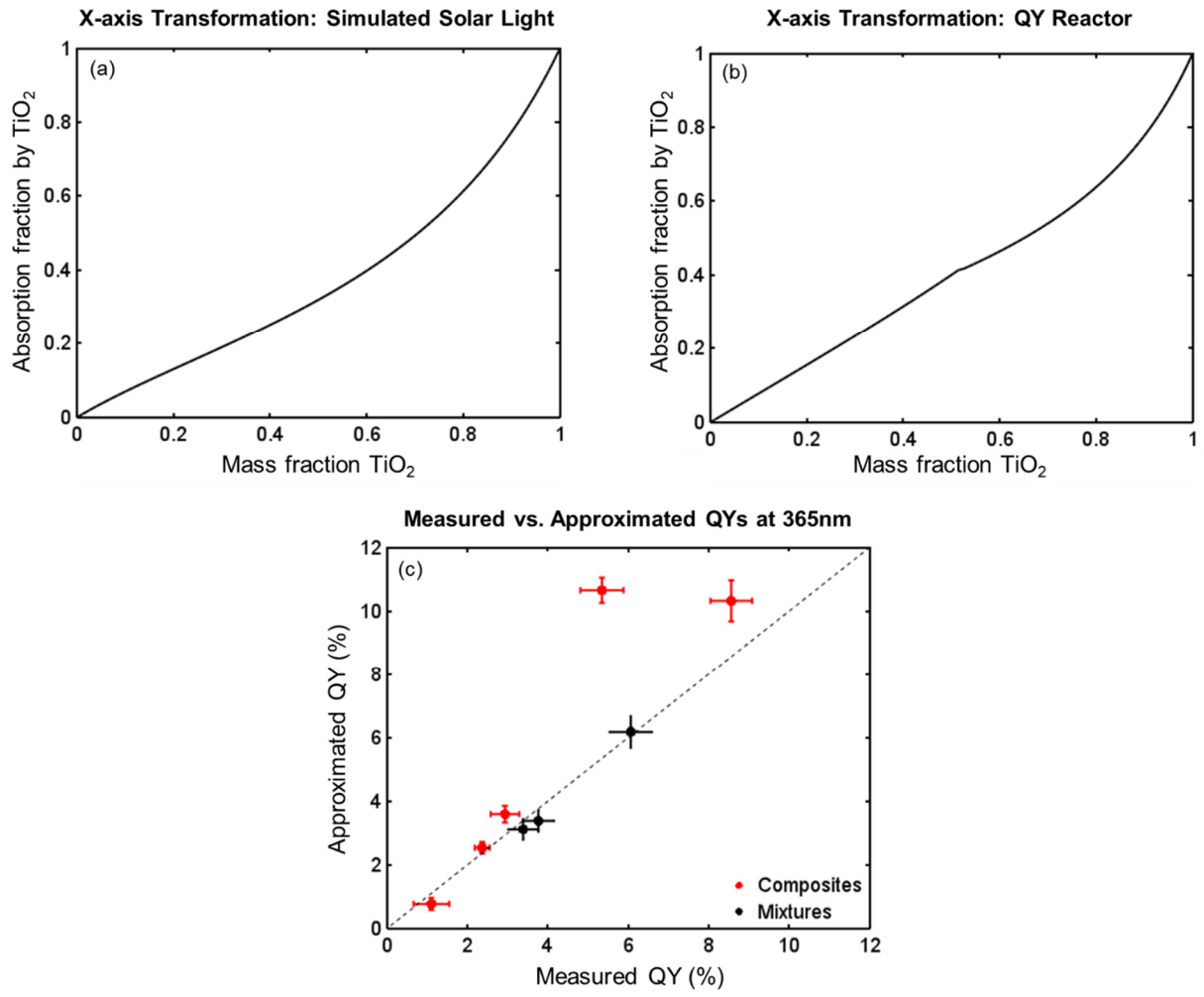

Figure S6. Transformation of the x-axis from mass fraction of TiO_2 to absorption fraction by TiO_2 according to equation (7), as it applies to data (a) using solar simulated light and (b) from the QY reactor with illumination at 365 nm. The kink in panel (b) results from the two-part fit of TiO_2 absorbance data in Figure S2c. (c) QYs were approximated for the experiments performed in the QY reactor and are compared to the measured QYs; the dotted line is a reference $y = x$ line, and error bars represent 95% confidence intervals. The two are seen to agree reasonably well. Note that some deviation is expected given that the path length of light is very short in this reactor, ~1 mm, resulting in deposition of catalyst particles along the reactor walls—primarily the inner reactor wall—over time; this deposition is expected to influence the QY approximation but have a minimal effect on the direct QY measurement.

More specifically, the absorbance measurements and fitting to Beer's law become less accurate as the particles deposit, making the QY approximation less accurate as well. This problem becomes apparent over longer time scales, which are required to reach steady-state. Since the g-C_3N_4 is very poorly dispersible, it is much more prone than TiO_2 to depositing on the reactor wall (which is visually observed). In a physical mixture of the two, the TiO_2 tends to remain dispersed while the g-C_3N_4 gradually deposits. However, in a composite, the g-C_3N_4 carries TiO_2 with it as it deposits on the inner reactor wall, thereby increasing the light intensity both components see and the amount

of light absorbed, increasing the approximated quantum yield relative to the actual one. Since pure TiO_2 is about an order of magnitude more active than pure g-C_3N_4, this effect becomes more pronounced with increasing TiO_2 content.

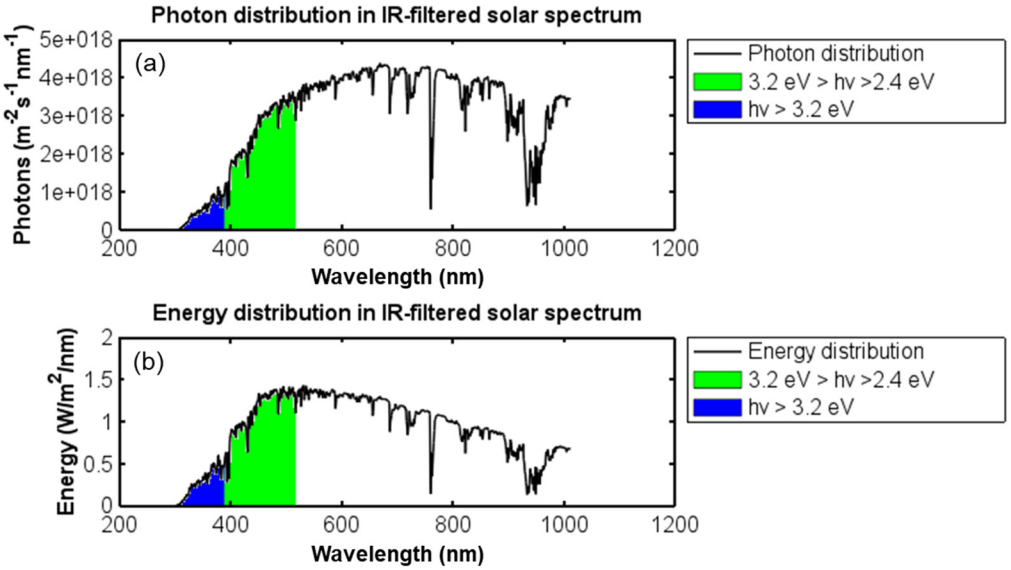

Figure S7. AM1.5 spectrum with a cut-off at 1013 nm, shown as both (a) a photon distribution and (b) an energy distribution. Green and blue shaded regions represent photons and energies available to a 2.4 eV band gap semiconductor and both a 2.4 eV and 3.2 eV band gap semiconductor respectively for absorption.

(a)

Assumptions		
Variables	**SC1**	**SC2**
Concentration	*free variable*	
Band gap	3.2 eV	2.4 eV
Abs. coeff.	5 cm^2/g	5 cm^2/g
Comp. QY	0.7	0.7

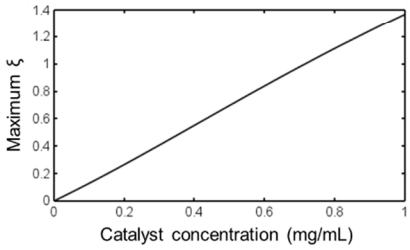

(b)

Assumptions		
Variables	**SC1**	**SC2**
Concentration	*free variable*	
Band gap	3.2 eV	3.2 eV
Abs. coeff.	5 cm^2/g	10 cm^2/g
Comp. QY	0.7	0.7

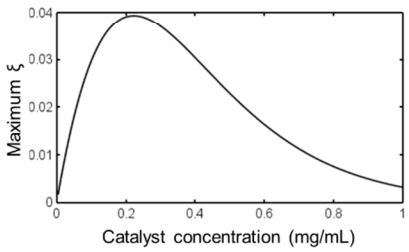

(c)

Assumptions		
Variables	**SC1**	**SC2**
Concentration	*free variable*	
Band gap	3.2 eV	3.2 eV
Abs. coeff.	5 cm^2/g	5 cm^2/g
Comp. QY	0.7	0.1

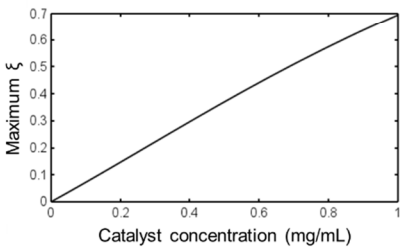

(d)

Assumptions		
Variables	**SC1**	**SC2**
Concentration	0.2 mg/mL	
Band gap	*free variable*	
Abs. coeff.	5 cm^2/g	5 cm^2/g
Comp. QY	0.7	0.7

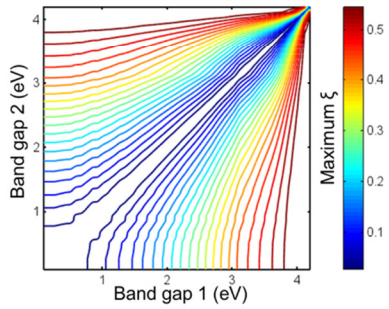

(e)

Assumptions		
Variables	**SC1**	**SC2**
Concentration	0.2 mg/mL	
Band gap	*free variable*	
Abs. coeff.	5 cm^2/g	10 cm^2/g
Comp. QY	0.7	0.7

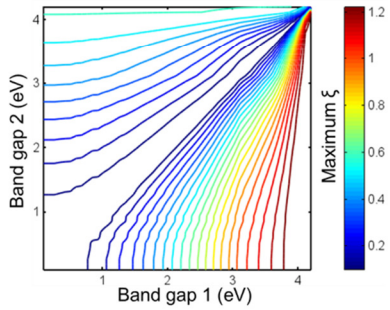

(f)

Assumptions		
Variables	**SC1**	**SC2**
Concentration	0.2 mg/mL	
Band gap	*free variable*	
Abs. coeff.	5 cm^2/g	5 cm^2/g
Comp. QY	0.7	0.1

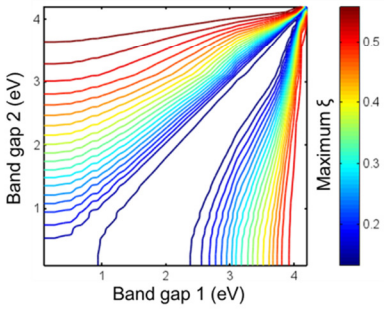

(g)

Assumptions		
Variables	**SC1**	**SC2**
Concentration	0.2 mg/mL	
Band gap	3.2 eV	2.4 eV
Abs. coeff.	*free variable*	
Comp. QY	0.7	0.7

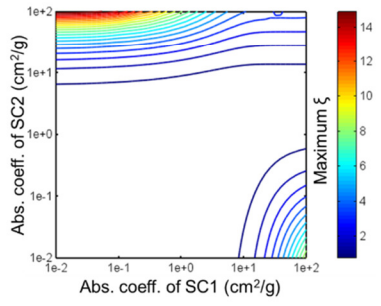

(h)

Assumptions		
Variables	**SC1**	**SC2**
Concentration	0.2 mg/mL	
Band gap	3.2 eV	3.2 eV
Abs. coeff.	*free variable*	
Comp. QY	0.7	0.7

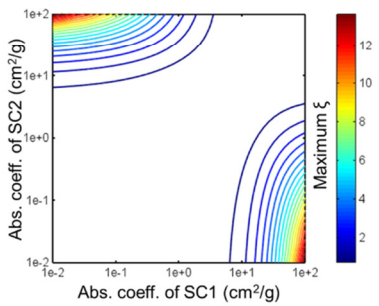

(i)

Assumptions		
Variables	**SC1**	**SC2**
Concentration	0.2 mg/mL	
Band gap	3.2 eV	3.2 eV
Abs. coeff.	*free variable*	
Comp. QY	0.7	0.1

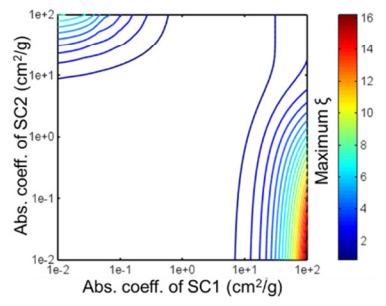

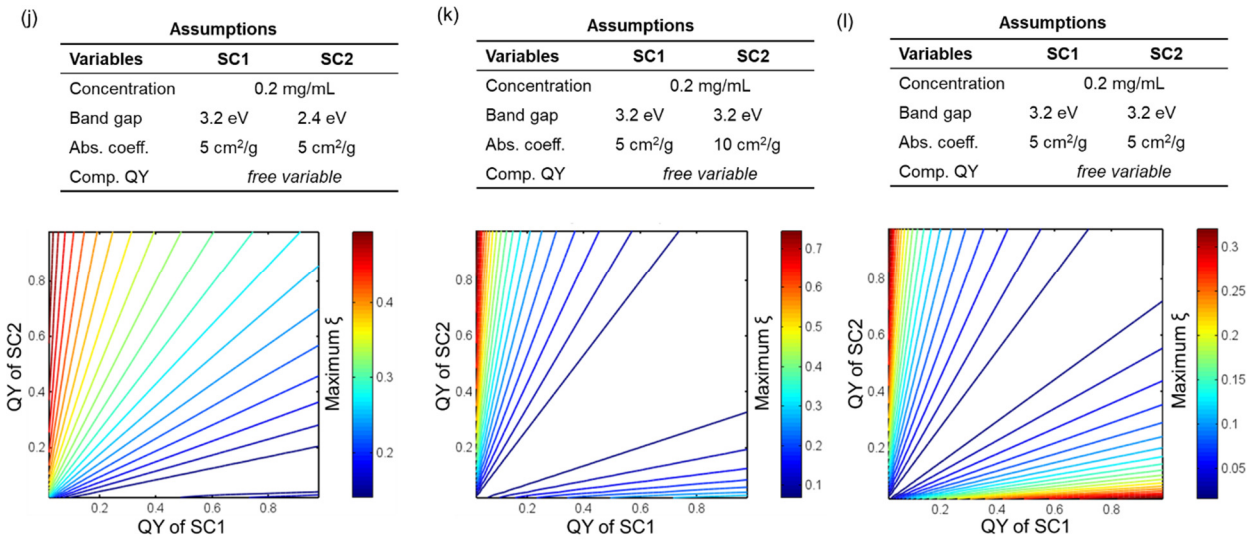

Figure S8. Detailed sensitivity analysis of the artificial enhancement introduced by mass-normalizing a two-photoabsorber no-enhancement model, showing covariance for each pair of input variables: concentration with (a) component band gaps, (b) component absorption coefficients, and (c) component quantum yields; band gaps with (e) absorbance coefficients and (f) quantum yields; absorbance coefficients with (g) band gaps and (i) quantum yields; and quantum yields with (j) band gaps and (k) absorbance coefficients. The redundancy in the covariance plots for the component properties consistently shows larger relative enhancement factors, for (1) the larger band gap material have the lower absorbance, (2) the larger band-gap material having the lower quantum yield, and (3) the material with the larger quantum yield having the larger absorbance coefficient. Covariance between individual component parameters - i.e., variance with (d) the band gaps of the two materials, (h) the absorbance coefficients of the two materials, and (i) the quantum yields of the two materials - are symmetric, as they should be.